(Received 2 January 2025, Accepted 3 February 2025, Scheduled 6 March 2025)

Fast Low Sidelobe Pattern Synthesis of Planar Arrays Having a Distorted Triangular or Rectangular Lattice Due to Row Displacements

Will P. M. N. Keizer*

I am retired and no longer working with The Physic Laboratory TNO
Oude Waalsdorperweg 63, 2597 AK, The Hague, The Netherlands

ABSTRACT: This paper describes the low sidelobe pattern synthesis of planar arrays having a distorted triangular or rectangular lattice. This distortion concerns variable row displacements applied to a triangular, skew or rectangular element lattice. The applied low sidelobe pattern synthesis is based on the iterative Fourier transform (IFT) method that makes extensive use of forward and inverse FFTs. Recently this author has developed new forward and inverse 2D FFT formulations. Due to these two new FFT formulations, the application of the IFT method is no longer limited to the pattern synthesis of a planar array having a rectangular lattice but can now also be applied to array apertures with a triangular or skew element lattice and even when such lattice has displaced element rows. The new IFT method is employed in this paper for the low sidelobe pattern synthesis of arrays featuring displaced element rows. The presented synthesized pattern results, which refer to the sum pattern, concern three planar arrays each with displaced element rows applied to a square or triangular lattice. The sum pattern of the considered antennas has to meet peak sidelobe level (PSLL) requirements for two nulling ring sectors, one of ≤ -50 dB and the other of ≤ -68 dB. The sum pattern of the third example includes a rectangular nulling sector specified by a PSLL of < -80 dB.

1. INTRODUCTION

In a recent paper [1], a new inverse 2D fast Fourier transform (FFT) was described that allows the calculation of the periodic array factor (AF) in cosine u-v space of planar array antennas featuring a triangular or skew element lattice. This new inverse 2D FFT can be directly applied to the original triangular element lattice without using an affine transformation that transforms a triangular or skew lattice into a square one [2]. In addition, a new forward 2D FFT was described in [1] that when being applied to the periodic AF, calculates the array element excitations related to a triangular or skew lattice. The IFT method using the new couple of 2D FFTs is successfully applied to the synthesis of various low sidelobe patterns of planar arrays having a triangular or skew lattice. The obtained results are described in [1]. The new couple of 2D FFTs makes that the IFT method of [1] is also applicable to the low sidelobe pattern synthesis of planar arrays featuring a distorted triangular or rectangular lattice if this distortion concerns variable row displacements.

In [3], the variable row displacement of planar array with a triangular lattice is shortly addressed, see pages 84–87. The reader is informed that lattice selections with proper variable row displacements applied to an original triangular lattice may give rise to the reduction of certain grating lobes within the specified scan sector. In [4], the same author describes the use of displaced columns instead of displaced rows to achieve a significant reduction of quantization lobes when those columns make use of subarrays. This technique allows wide angle scanning in the azimuth plane and narrow scanning in the elevation plane. Paper [4] is a follow up of an earlier paper [5] using the same approach as described in [4].

This paper presents for the first time synthesized low sidelobe pattern results for arrays having a distorted rectangular or rectangular lattice. These results, obtained with the IFT method of [1], refer to three different array configurations. These three results deal with the sum pattern and are all designed for two ring sectors of which one features a ≤ -50 dB PSL requirement and the other ≤ -68 dB. The third example deals also with two ring sector requirements and includes furthermore a -80 dB PSLL rectangular nulling sector.

As far as known, there has never been a paper published about the low sidelobe pattern synthesis of array antennas with a rectangular or triangular lattice featuring displaced element rows.

Array apertures with distorted rectangular or triangular lattices caused by row or column displacements are suitable for phased array radar systems with a limited scan capability in the azimuth or elevation plane and a wide scan range for the other orthogonal, elevation or azimuth plane. Candidates are precision approach radars.

2. DISTORTED TRIANGULAR LATTICE

Figure 1 shows the element locations of a planar array aperture having a triangular element lattice. All odd numbered rows feature the same displacement $\Delta_n = 0.5$ while for the even num-

* Corresponding author: Will P. M. N. Keizer (willkeizer@ieee.org).

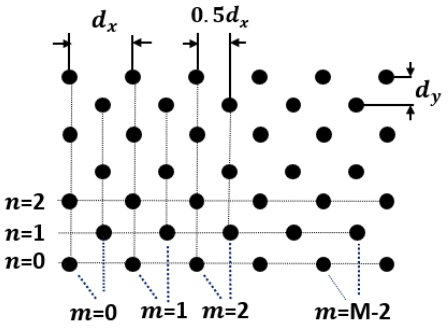

FIGURE 1. Triangular element lattice (originally published in [1]).

bered rows Δ_n is equal to $\Delta_n = 0$. The elements in the same row have an inter-element spacing of d_x. The vertical spacing between two successive rows is d_y.

The equation of AF in u-v space valid for the triangular lattice of Fig. 1 is given by

$$F(u,v) = \sum_{m=0}^{M-1}\sum_{n=0}^{N-1} A_{mn} e^{jk[(m+\Delta_n)d_x u + n d_y v]}$$

$$\Delta_n = 0.5 \text{ for } n = \text{odd}, \ \Delta_n = 0 \text{ for } n = \text{even or } 0 \quad (1)$$

where A_{mn} is the excitation of element (m,n), k the wavenumber $(2\pi/\lambda)$, and λ the wavelength. In (1), u and v are the direction cosines $u = \sin\theta\cos\varphi$ and $v = \sin\theta\sin\varphi$ with θ being the elevation angle.

The preceding part of Section 2, including Fig. 1 and Equation (1), is replicated from [1].

When the row displacement in Fig. 1 for every row is equal to $\Delta_n = 0$, the triangular lattice becomes a rectangular one. One obtains a skew lattice when the row displacement varies according to $\Delta_n = n * \text{del}$ with del in the range of $-1 < \text{del} < 1$.

This paper deals with the low sidelobe pattern synthesis of planar arrays where the extent of the row displacement varies from row to row. The array configuration is as shown in Fig. 1, but the rows feature different distances Δn not related to those of a triangular or skew lattice.

2.1. Used IFT Method

The low sidelobe pattern synthesis used in this paper is the same IFT method as described in [1] and relies on the use of the new developed couple of inverse and forward 2D FFTs. The MATLAB formulation of the inverse 2D FFT to calculate the array factor, designated by *AFuv*, for direction cosine u-v space is included in Appendix A of [1]. The MATLAB formulation of the forward 2D FFT suitable for the computation of the corresponding element excitations from *AFuv* is based on Equations (18)–(21) in [1].

The aperture positions of the array elements of a planar array arranged along a distorted triangular or rectangular lattice caused by row displacements lack any periodicity. The consequence of this deficiency is that its *AFuv* in u-v space has no periodicity along the u-direction caused by random row displacements but still has periodicity along the v-direction. However, array factors of array antennas with a rectangular, triangular, or skew lattice are all characterized by a double periodicity in u-v space due to the double periodicity of their element positions along the array aperture.

The shape of *AFuv* in u-v space of an array with a distorted triangular or rectangular lattice calculated by the inverse 2D FFT formulated in [1] is always a rectangle one. The u-v coordinates of *AFuv* are positioned in the range,

$$-\frac{\lambda}{2d_x} \le u \le \frac{\lambda}{2d_x} \quad (2)$$

$$-\frac{\lambda}{2d_y} \le v \le \frac{\lambda}{2d_y} \quad (3)$$

The area of *AFuv* has a width in the u-direction of λ/d_x and a height λ/d_y along the v-direction as directly follows from (2) and (3).

When the calculation of *AFuv* is made for $K \times K$ directions in u-v space, their u-positions, according to new inverse 2D FFT formulation of [1], follow from

$$u_p = \frac{p}{K}\frac{\lambda}{d_x} \quad p = -\frac{K}{2}\ldots\frac{K}{2} - 1 \quad (4)$$

and the corresponding v-positions are equal to

$$v_q = \frac{q}{K}\frac{\lambda}{d_y} \quad q = -\frac{K}{2}\ldots\frac{K}{2} - 1 \quad (5)$$

with $K \ge$ next power of 2 for $\log 2(4\text{x maximum}(M,N))$.

Equations (2)–(5) are applied to rectangular, triangular, and skew aperture element lattices and also when these lattices are distorted by displaced rows.

2.2. Periodicity of AFuv

Any *AFuv* characterized by random row displacements lacks double periodicity but is still periodic in v-direction despite the absence of any periodicity of the element positions. Since the periodicity of *AFuv* is restricted to the v-direction, *AFuv* repeats itself only in the v-direction. The absence of double periodicity for *AFuv* means that parts of AF in u-v space without periodicity or not located in the area of *AFuv*, having the size of $\lambda^2/(d_x d_y)$, are not involved in the pattern synthesis performed by the IFT method. For those parts of AF, the sidelobe level remains undefined. This problem is absent for array apertures having a rectangular, triangular, or skew element lattice. Such array apertures feature a double element periodicity and therefore also double periodicity for the array factor *AFuv* [6].

2.3. The Strategy Used to Prevent Trapping with the IFT Method

The best strategy to eliminate trapping during the low sidelobe synthesis of the sum pattern is to select, as taper at the start of the synthesis, the uniform one which features the narrowest main beam width together with the highest sidelobes. Since each iteration of the IFT method causes a decrease of the peak sidelobe level of its pattern, a repeated widening of the

main lobe is inevitable. Therefore, at each iteration of the IFT method, new positions of the main beam nulls in u-v space are computed to determine which far-field directions of *AFuv* are contained in the main lobe region and which ones belong to the sidelobe region. Far-field directions of the main lobe are not involved in the pattern synthesis. Only samples of the sidelobe region of *AFuv* are adapted to the sidelobe requirements.

The used IFT method employs a simple MATLAB function that calculates, during each iteration, the precise extent of the null border of the *AFuv* main lobe footprint in u-v space. The absence of any requirement for the size of the main lobe nulling region in u-v space, combined with the use of the uniform taper as initial taper followed by performing frequent recalculations of the main beam nulling contour, ensures that the IFT method is not affected by trapping.

3. SYNTHESIZED RESULTS

The low sidelobe pattern synthesis concerns three different array antenna configurations each having row displacements. Only sum patterns are synthesized with the main beam pointing at broadside. The first two examples deal with the synthesis of an amplitude-only taper and involves the nulling of two ring sectors. The third example concerns the synthesis of a complex-amplitude taper and deals with the nulling of two ring sectors in combination with the nulling of a single rectangular sector.

The applied array aperture for the three array configurations has, in absence of any row displacement, a square shape with a width and height both equal to 0.4 m. The operating frequency is 10 GHz.

3.1. Example 1

This example consists of a planar array occupied with 484 elements arranged along 22 rows and 22 columns. The column d_x spacing between two successive elements in a row is equal to 0.0180 m, and the spacing d_y between two successive rows amounts to 0.0180 m. The initial lattice is a square one. This lattice is distorted by the displacement of the first row # 1 and the last row # 22 over a distance equal to 0.0108 m to the right.

The low sidelobe synthesis involves two nulling ring sectors. Ring sector 1 has an outer radius equal to 0.4 in u-v space while its inner "radius" coincides with the u-v null positions of the main lobe. This ring sector includes all *AFuv* directions located within ring sector 1 according to $u^2 + v^2 < 0.40^2$, except the ones of the main lobe region. The null positions of the main lobe region are updated during each iteration of the synthesis. The PSLL requirement for ring sector 1 is ≤ -50 dB. Ring sector 2 comprises all sidelobe *AFuv* directions from the outer radius 0.4 of ring sector 1 up to the border of the *AFuv* area. Therefore, an outer radius of 1.18 is used for ring sector 2 to assure that all sidelobe directions of *AFuv*, including those located in invisible u-v space, participate in the pattern synthesis, see Section 4. PSLL for ring sector 2 is specified as ≤ -68 dB.

Figure 2 shows the convergence rate of the synthesis with respect to the two PSLLs. The low sidelobe synthesis matches the specified PSLL requirements after 1432 iterations. The execution time of the synthesis was only of the order of 0.99 s.

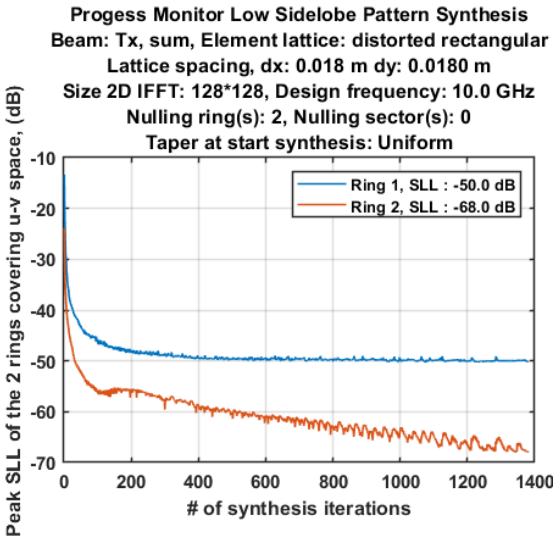

FIGURE 2. Convergence rate of low sidelobe synthesis of the sum pattern using the IFT method. Example 1.

The computation of *AFuv* during the IFT pattern synthesis was conducted with a resolution for $K \times K$ of 128×128, see Fig. 2.

Figure 3(a) shows the normalized AF pattern for whole visible u-v space. Fig. 3(b) shows the corresponding peak sidelobe distribution. Fig. 4(a) visualizes the principal u-cut of the pattern of Fig. 3(a). Fig. 4(b) does this for the principal v-coordinate. It can be noticed from Fig. 4(a) that a limited number of u-directions of AF with $|u| > 0.8333$ slightly exceed the PSLL ≤ -68 dB requirement.

Figure 5(a) shows the principal u-cut of the main beam of Example 1 when being scanned to the angular position $\theta = 15°$, $\varphi = 15°$ at the frequency 10 GHz. Fig. 5(b) shows the principal v-cut of the same scanned beam. Phase scanning of the main beam of a phased array antenna obeys the Fourier shift property. Due to this property, the shape of the main beam and also those of the sidelobes are not changed during scanning [7].

The reason for this is that these directions are not part of *AFuv* and therefore were not involved in the low sidelobe synthesis of the IFT method. Fig. 6 shows the scanned array pattern to the position $\theta = 10°$, $\varphi = 60°$. No grating lobe is visible. However, when the main beam is scanned to the angular position $\theta = 80°$, $\varphi = 130°$, some grating lobes show up in visible u-v space as displayed in Fig. 7. The element amplitude distribution responsible for the antenna pattern results of Fig. 3(a) is shown in Fig. 8. In this figure, one can notice the presence of reverse tapering near at least the two corners $\{x = -0.2, y = 0.2\}$ and $\{x = 0.2, y = -0.2\}$ of the aperture of Example 1. Reverse tapering at the aperture periphery is typical for Tsjebysjev tapers which are characterized by uniform peak sidelobes. To get an idea about the impact of displaced rows on the array radiation performance, the array factor is calculated for the original square aperture lattice with $d_x = d_y = 0.018$ m in the absence of any row displacement. This array factor is synthesized using the same peak low sidelobe requirements as for Example 1. After the synthesis, the main beam is scanned to the position $\theta = 80°$, $\varphi = 130°$. The impact of this scanning on the array factor is depicted in Fig. 9.

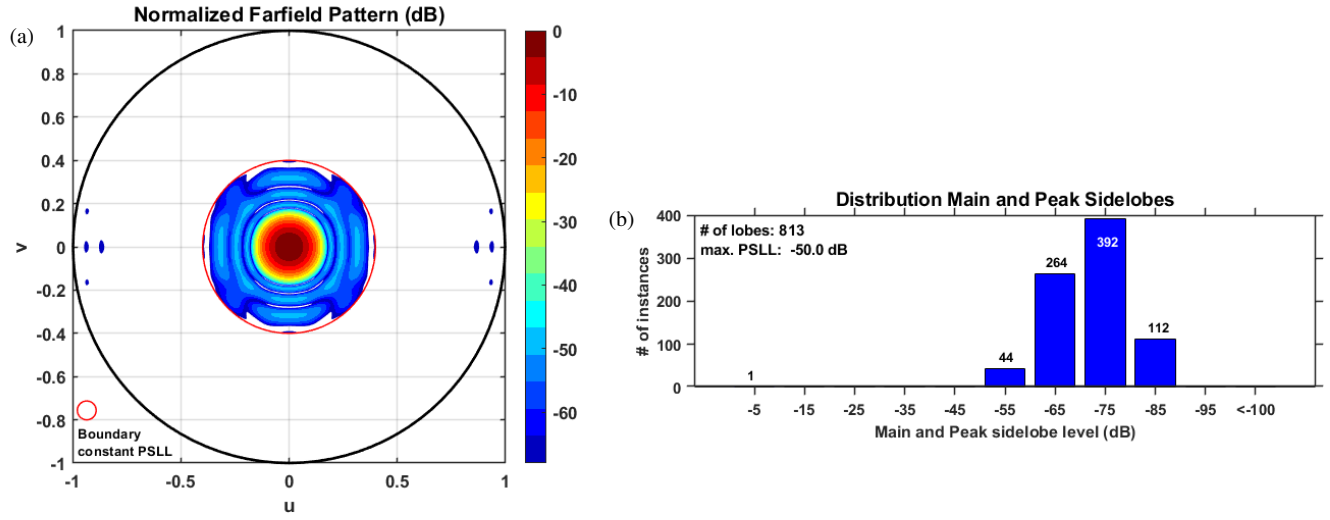

FIGURE 3. (a) Pseudo contour of the normalized array factor of the synthesized sum pattern. (b) Corresponding peak sidelobe distribution for whole visible u-v space. Example 1.

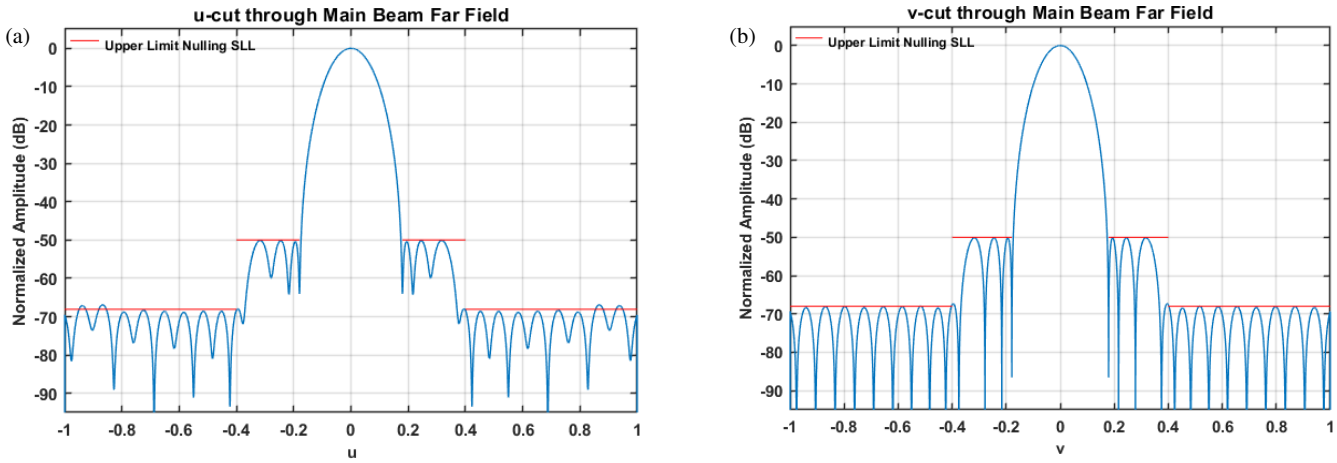

FIGURE 4. Principal u-cut of the array factor pattern shown in Fig. 3(a). Principal v-cut of the array factor pattern shown in Fig. 3(a).

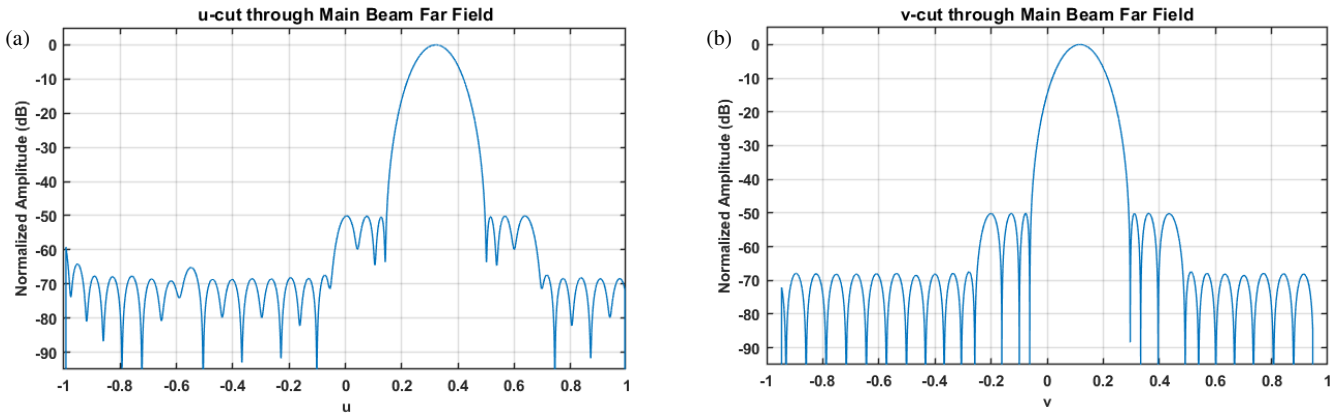

FIGURE 5. (a) Principal u-cut of the array factor shown in Fig. 3(a) when the main beam is scanned to the angular position $\theta = 15°$, $\varphi = 15°$. Frequency $= 10$ GHz. Example 1. (b) Principal v-cut of the array factor shown in Fig. 3(a) when the main beam is scanned to the angular position $\theta = 15°$, $\varphi = 15°$. Frequency $= 10$ GHz. Example 1.

By comparing the array factor of Fig. 9 with that of Fig. 7 which has two row displacements, one can see that these displaced rows are responsible for the presence of the parasitic grating lobes near $u = 0.85$, $-0.42 < v < 0.4$.

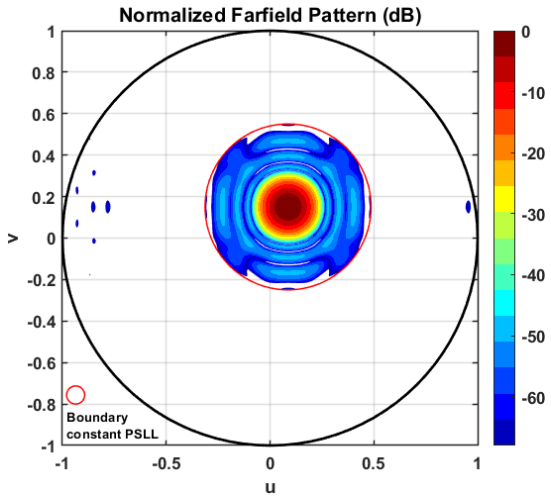

FIGURE 6. Array factor with the main beam scanned to the angular position $\theta = 10°$ and $\varphi = 60°$. Example 1.

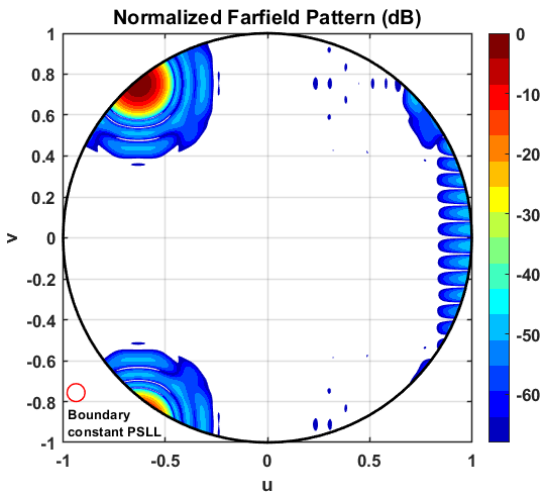

FIGURE 7. Array factor with the main beam scanned to the angular position $\theta = 80°$ and $\varphi = 130°$. Example 1.

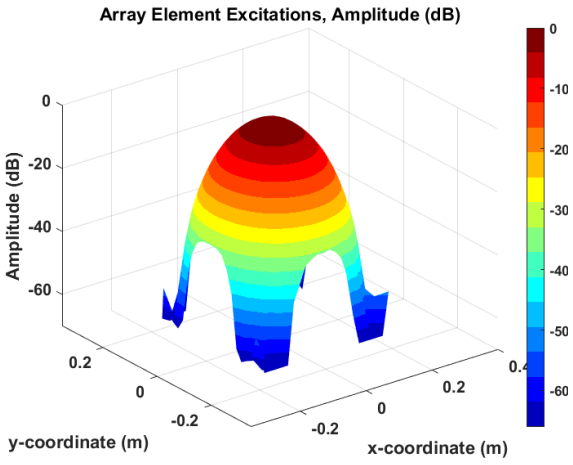

FIGURE 8. Array element amplitude distribution responsible for the array pattern of Fig. 3(a). Example 1.

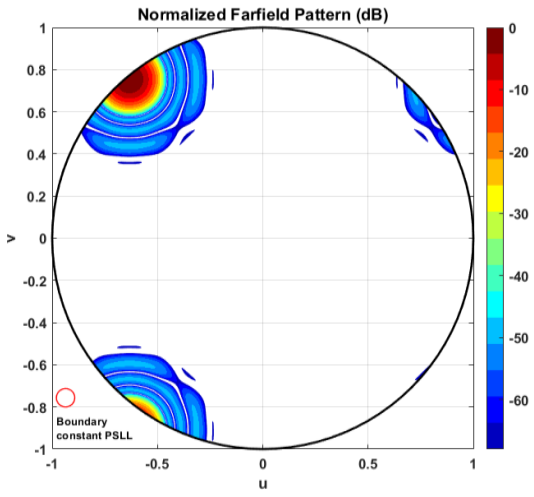

FIGURE 9. Array factor with the main beam scanned to the angular position $\theta = 80°$ and $\varphi = 130°$. This array factor refers to the original square lattice in absence of any row displacement but with the same sidelobe requirements as for Example 1 during the low sidelobe synthesis.

Figure 10 illustrates the element positions across the array aperture having two horizontally displaced element rows; one of these rows is located at the bottom of the aperture and the other row at top of the aperture.

3.2. Example 2

The second example starts with the same initial square array element lattice as used for Example 1 and is therefore equipped with 484 elements distributed over 22 rows and 22 columns. The element spacings are also identical and are therefore $d_x = 0.0180\,\text{m}$ and $d_y = 0.0180\,\text{m}$.

The used lattice distortion compromises the displacement of 6 rows with the odd numbers 1, 3, 5, 7, 8, 11 over a distance $-0.009\,\text{m}$. The positions of the remaining 16 rows with the even numbers 2, 4, 6, 8, 10, 12–22 are not changed as shown in Fig. 11. Due to this choice of row displacements, the aperture of Fig. 11 deals with two element lattice types. The first 11 top rows constitute a triangular element lattice. The next 11 rows are part of the original undistorted square lattice.

The low sidelobe synthesis involves two nulling ring sectors. The radius of the outer ring of ring sector 1 is equal to 0.45 while the inner ring of this nulling sector coincides with the null positions of the main lobe. These main lobe null positions are updated during each iteration of the low sidelobe synthesis. The PSLL requirement for the nulling ring sector 1 is $\leq -50\,\text{dB}$. The PSLL for ring sector 2 is specified as $\leq -68\,\text{dB}$. For its outer ring, the radius is specified as 1.18 to take all directions of $AFuv$ in u-v space into account including those located in invisible u-v space. Fig. 12 shows the convergence rate of the two PSLLs. The low sidelobe synthesis matches the two specified PSLL requirements after 717 iterations. The execution time of the synthesis was of the order of 0.43 seconds. Fig. 13(a) shows the normalized AF pattern for the whole visible u-v space. Fig. 13(b) shows the corresponding peak sidelobe distribution for the whole visible u-v space. Fig. 14 visualizes the principal u-cut of the pattern of Fig. 13(a). Fig. 15 displays the

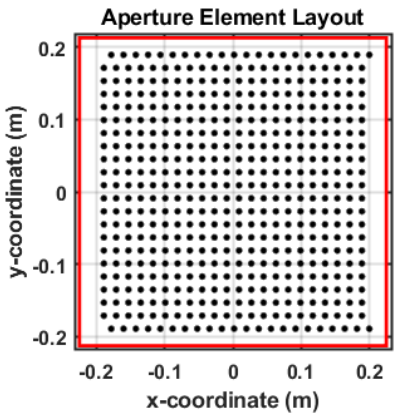

FIGURE 10. Array aperture element positions showing the distorted rectangular lattice. Example 1.

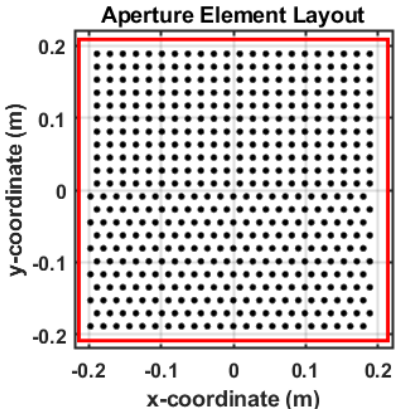

FIGURE 11. Array aperture element positions showing the distorted rectangular lattice caused by the six row displacements. Example 2.

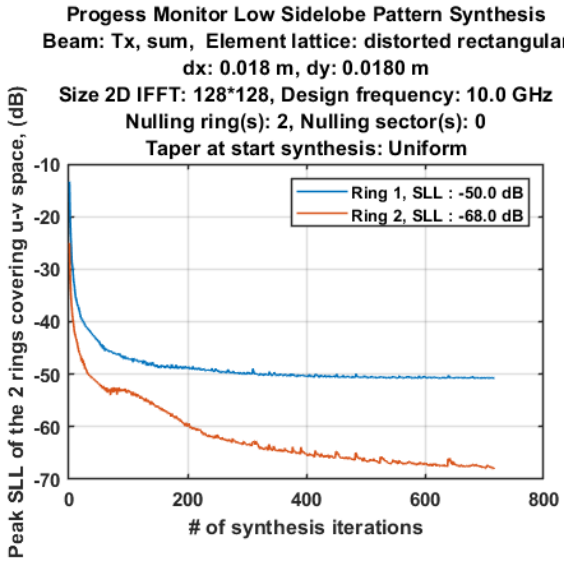

FIGURE 12. Convergence rate of low sidelobe synthesis of the sum pattern using the IFT method. Example 2.

array pattern with the main beam scanned to the angular position $\theta = 10°$, $\varphi = 60°$. No grating lobes are visible. However, when the main beam is scanned to the angular position $\theta = 80°$, $\varphi = 130°$, various parasitic grating lobes show up in visible u-v space as shown by Fig. 16. The array factor of this figure shows more pronounced parasitic lobes than the array factor of Fig. 7, Example 1. Likewise, as for Example 1 one can also notice for Example 2, by inspecting Fig. 14, that for u-directions with $|u| > 0.8333$ the PSLL ≤ -68 dB requirement is violated. This is also confirmed by the array pattern of Fig. 13(a). However, for directions with $|v| > 0.8333$, any violation of the PSLL ≤ -68 dB requirement is absent. Responsible for this is the periodicity of *AFuv* in the v-direction.

3.3. Example 3

The third example starts with a triangular array element lattice aperture consisting of 640 elements distributed over 32 rows and 20 columns. The spacing between the two neighboring elements on the same row is $d_x = 0.020$ m, and the spacing between the rows is $d_y = 0.0125$ m. The applied variable row displacement in the x-direction concerns all rows and has a random nature for every row. The maximum row displacement is 0.0526 m, and its minimum value is equal to -0.0405 m. Fig. 17 shows the element positions of the array aperture with the displaced rows as applied to Example 3.

The low sidelobe synthesis for u-v space involves two ring sectors with different PSLL requirements. Ring sector 1 has an outer radius equal to 0.50 while the inner radius coincides with the null positions of the main lobe. The PSLL requirement for ring sector 1 is ≤ -50 dB. The ring sector 2 contains all u-v directions of the rectangular non-periodic *AFuv* except those of ring sector 1 and the ones of the main lobe. Also, for Example 3, the PSLL for ring sector 2 is specified as ≤ -68 dB. The low sidelobe synthesis furthermore involves a nulling rectangular sector with u-v dimensions $\{0.6 \leq u \leq 0.68, \text{ and } -0.1 \leq v \leq 0.3\}$ of which the PSLL specification is equal to ≤ -80 dB.

Figure 18 shows the convergence rate for the three PSLL requirements. The low sidelobe synthesis matches the three specified PSLLs after 947 iterations. This result was obtained within 0.77 s execution time of the synthesis. Fig. 19(a) shows the normalized AF pattern for the whole visible u-v space. Fig. 19(b) does this for its associated peak sidelobe distribution. Fig. 20 visualizes the principal u-cut of the pattern of Fig. 19(a). As one can see from Fig. 19(a) and Fig. 20, the PSLL level of the rectangular nulling sector fully matches the specification of < -80.1 dB. The synthesis of this nulling sector is feasible because its location is fully covered by the area of *AFuv*. Fig. 21 shows the pattern with the main beam scanned to $\theta = 10°$, $\varphi = 60°$. Like the other Examples 1 and 2, this scanned pattern is not corrupted by parasitic grating lobes. In Fig. 22 where the main beam is scanned to the position $\theta = 80°$, $\varphi = 130°$, various parasitic grating lobes are visible however with lower peak values than the peak of the scanned main lobe.

The results for the three examples confirm the observation made in [3] that when rows of a triangular element lattice are subjected to variable displacements, it can impact and create parasitic grating lobes. These impacts concern possible

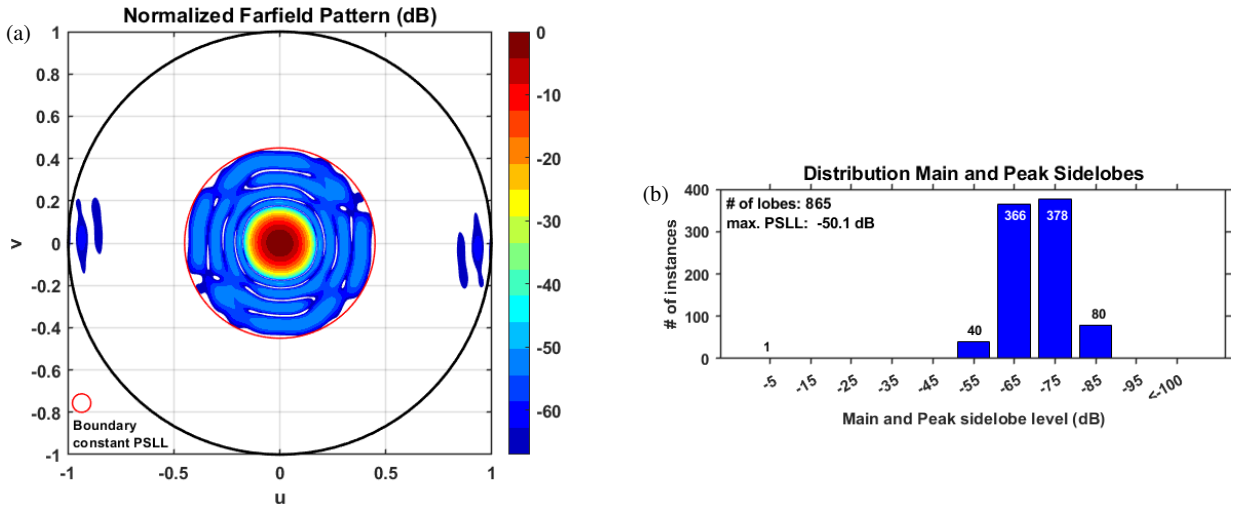

FIGURE 13. (a) Pseudo contour of the normalized array factor of the synthesized sum pattern. (b) Corresponding peak sidelobe distribution for whole visible u-v space. Example 2.

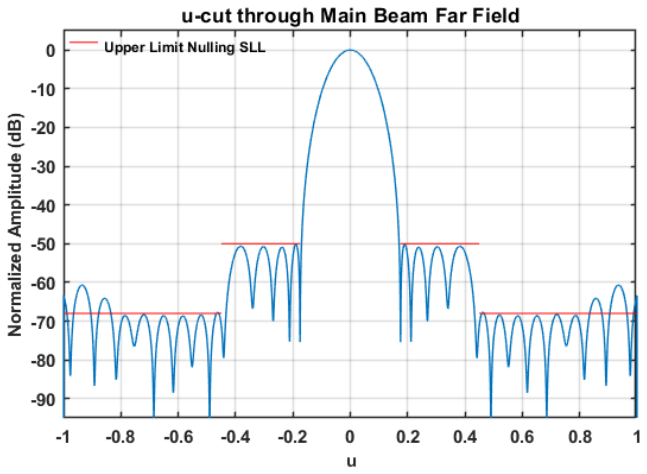

FIGURE 14. Principal u-cut of the array pattern shown in Fig. 13(a). Only the sidelobes for $|u| > 0.8333$ do not match the PSLL requirement. Example 2.

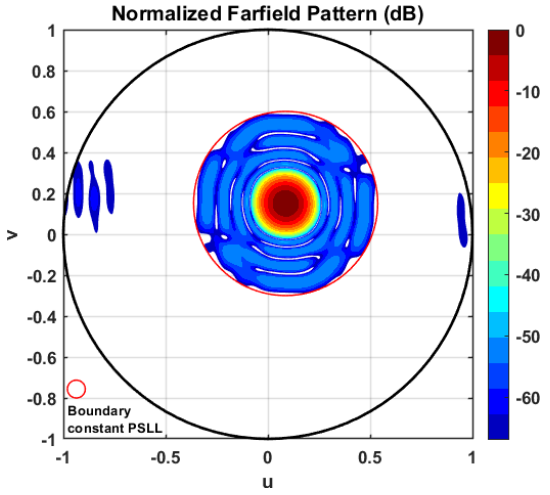

FIGURE 15. Array factor with the main beam scanned to the angular position $\theta = 10^\circ$ and phi $= 60^\circ$. The array factor refers to Example 2.

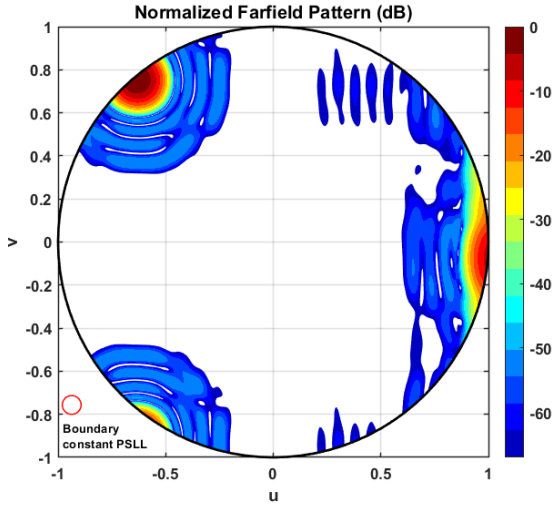

FIGURE 16. Scanned array factor to the angular position $\theta = 80^\circ$ and phi $= 130^\circ$. The array factor refers to Example 2.

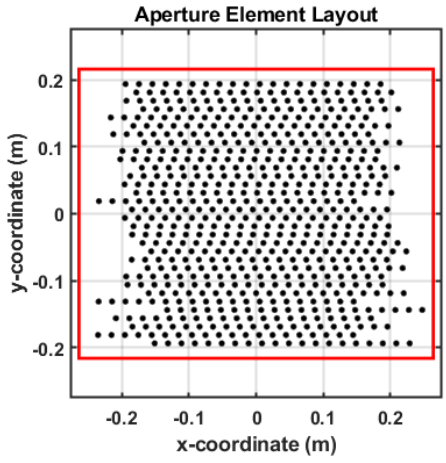

FIGURE 17. Array aperture element positions showing the distorted triangular/rectangular lattice due to the random, variable row displacements. Example 3.

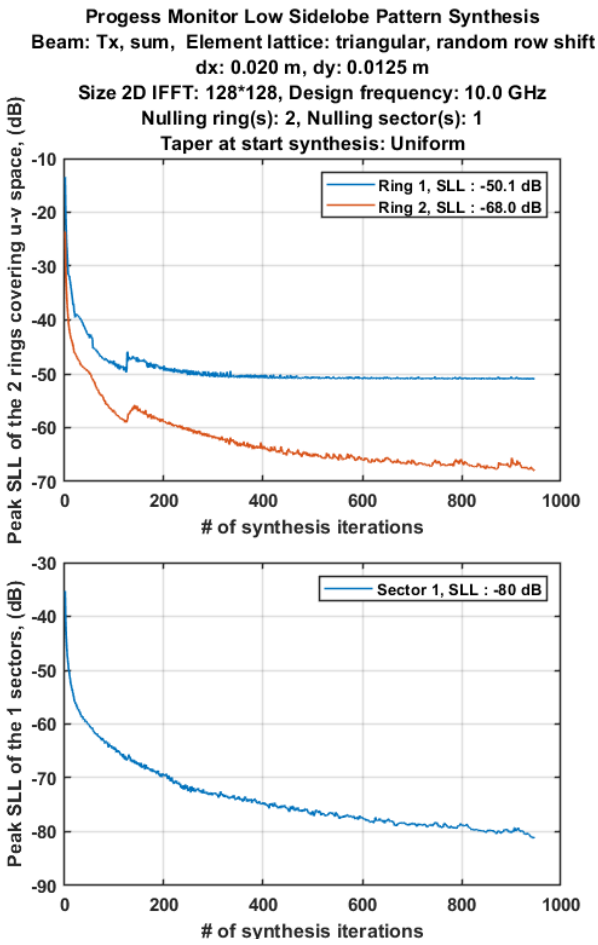

FIGURE 18. Convergence rate of low sidelobe synthesis of the sum pattern using the IFT method. Example 3.

changed positions in u-v space and likely reductions of their peak values. Both phenomena have been seen with the three examples described in this paper.

4. RESTRICTIONS OF THE IFT METHOD

Using the IFT method, it is not always guaranteed for planar array antennas having variable row displacements that all directions of AF located in visible u-v space are involved in low sidelobe pattern synthesis when the original lattice is a rectangular or triangular one. Responsible for this shortcoming is the lack of periodicity in the u-direction for *AFuv* caused by the variable row displacements and occurs when the width of *AFuv* in the u-direction is < 2. Fig. 23 shows the extent of *AFuv* in u-v space of Examples 1 and 2 for the main beam positioned at broadside. The yellow colored square section in this figure represents the area of *AFuv*. The two green colored square blocks, labeled by letters A and D, are each a full replica of *AFuv* because of its periodicity in the v-direction. No replicas are present left and right of *AFuv* due to the lack of periodicity in the u-direction. The lack of these two replicas is the reason that the two narrow, small white areas enclosed by the red colored circle (radius $= 1$) are excluded from the low sidelobe synthesis using the IFT method. This explains why in these two areas the peak

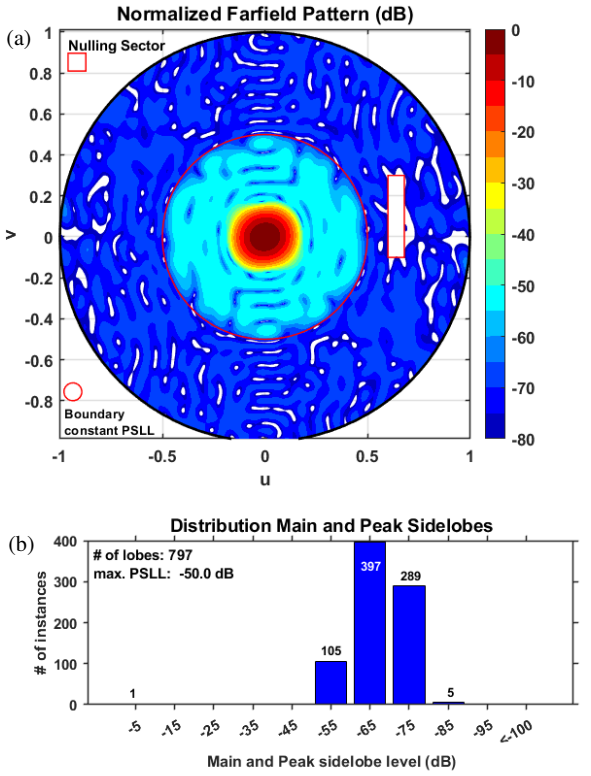

FIGURE 19. (a) Pseudo contour of the normalized array factor of the synthesized sum pattern. (b) Corresponding peak sidelobe distribution for whole visible u-v space. Example 3.

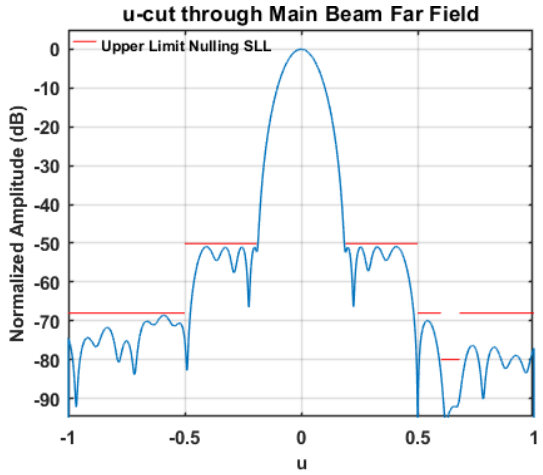

FIGURE 20. Principal u-cut of the array pattern shown in Fig. 19(a). Example 3.

values of some sidelobes exceed > -68 dB. In case that the width of *AFuv* satisfies $\lambda/d_x \geq 2$, all far-field directions of the whole visible u-v space can be involved in the IFT synthesis. The four yellow (triangle) parts, found outside the red colored circle and situated close to the four corners of *AFuv*, take part in the synthesis through the nulling ring sector 2 because its outer ring radius is equal to 1.18.

The same arguments as for Examples 1 and 2, with respect to limitations of the IFT method just mentioned, apply equally to Example 3.

TABLE 1. Array performance at broadside scan for the synthesized sum taper.

Example	# of elements	Size aperture	Dir (dB)	3 dBu	3 dBv
1	484	0.4 m × 0.4 m	29.68	0.1118	0.1117
2	484	0.4 m × 0.4 m	29.84	0.1094	0.1101
3	640	0.4 m × 0.4 m	29.61	0.1158	0.1085
1a*	484	0.4 m × 0.4 m	29.70	0.1115	0.1116

Legend 1a* = Example 1 without row displacements

TABLE 2. Array performance at broadside scan for the uniform sum taper.

Example	# of elements	Size aperture	Dir (dB)	3 dBu	3 dBv
1	484	0.4 m × 0.4 m	33.16	0.0672	0.0672
2	484	0.4 m × 0.4 m	33.23	0.0671	0.0672
3	640	0.4 m × 0.4 m	33.32	0.0653	0.0665
1a/2a*	484	0.4 m × 0.4 m	33.37	0.0671	0.0671

Legend 1a/2a* = Examples 1+2 without row displacements

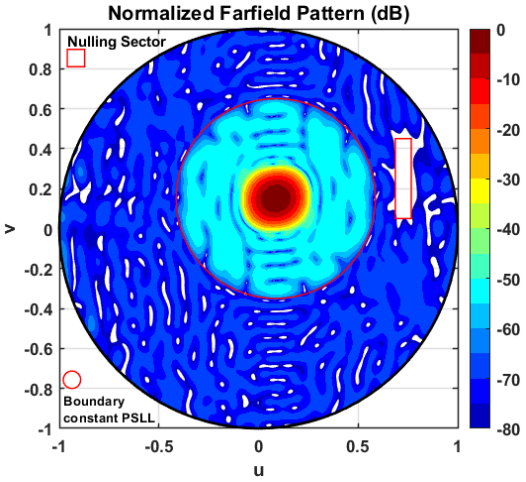

FIGURE 21. Array factor with the main beam scanned to the angular position $\theta = 10°$ and phi $= 60°$. The array factor refers to Example 3.

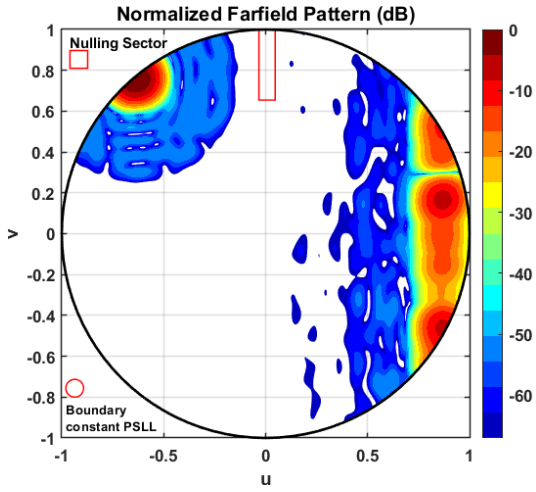

FIGURE 22. Pseudo contour plot of the normalized array factor with the main beam scanned to the angular position $\theta = 80°$, phi $= 130°$. Example 3.

5. OVERVIEW OF THE SYNTHESIZED RESULTS

Tables 1, 2, and 3 inform about synthesized results using the IFT method for the three examples described. The used low side-lobe synthesis refers to the sum pattern. For all three considered examples, the shape of the aperture was almost a square one about 0.2 m high and 0.2 m wide. Table 1 shows the computed directivity, symbol Dir, and the computed 3 dB beamwidth, for the principal u- and v-planes indicated by the symbols "3 dBu" and "3 dBv", respectively. One can see that for all three examples, directivities are almost equal. Same remark applies to the 3 dB beamwidth results. Table 2 shows the computed results in case that the applied sum taper is the uniform one, and no synthesis is applied. From the directivities shown in Tables 1 and 2, one is able to derive what the aperture efficiency is for each of the three examples. Table 3 gives an overview of the number of iterations and execution times used by the IFT method to get the results shown in Table 1. For each of the three Examples, the execution time was less than 1 second.

TABLE 3. Overview of the execution time and number of iterations used by the IFT method for the pattern synthesis of the three examples.

Example	# of elements	Execution time (s)
1	1432	0.99
2	717	0.43
3	947	0.76

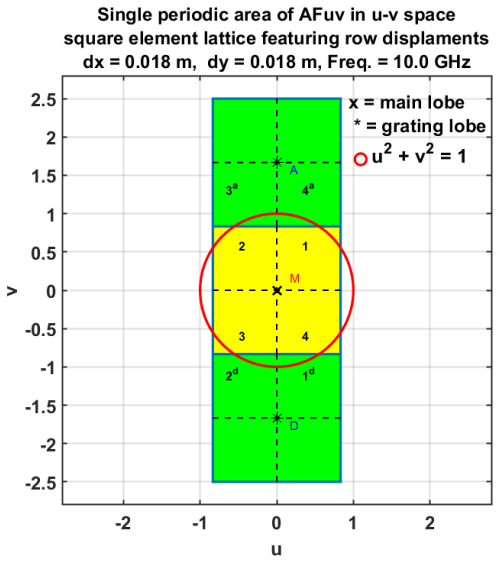

FIGURE 23. Single periodic area of *AFuv* in u-v space. The two green colored square blocks are each a full replica of *AFuv* due to its periodicity in v-direction. The main beam is positioned at broadside. This figure refers to the *AFuv's* of Examples 1 and 2.

6. CONCLUSIONS

The IFT method described in [1], using the new set of inverse and forward FFTs suitable for the low sidelobe synthesis of array antenna with double periodic spaced antenna elements, has been successfully applied to the low sidelobe pattern synthesis of arrays with a distorted triangular or rectangular lattice. The presented synthesized results apply to three different array configurations. These results show that the specified low sidelobe requirements have almost been fully met within short computation times and were not hampered in any way from trapping as shown by Figs. 2, 12, and 19. For each of the three presented examples, the computation of the synthesis required less than 1 second. That the pattern synthesis was not completely successful with respect to the specified PSLL's is related to disrupting the periodicity of *AFuv* in the u-direction caused by the used row displacements.

That variable displacements of the rows can affect the position of parasitic grating lobes, as mentioned in [3], has been confirmed. In papers [4, 5], it was shown that column displacements, which have the same impact as row displacements, can improve scan range. However, the present results show that array antennas with a rectangular or triangular element lattice and using row displacements lack a wide scan capability in the two orthogonal dimensions. The absence of the wide scan capability in two dimensions is related to the used d_x and d_y spacings for Examples 1 and 2 which are both equal to 0.6λ. Such spacings exclude a wide scan capability in elevation and azimuth. Example 3 features an element spacing $d_y = 0.4167\lambda$ and 0.6667λ for d_x. These spacing values mean a large scan capability in elevation for this example but a reduced one for azimuth.

It should be noted that the purpose of the research described in this paper is to investigate whether the synthesis of low sidelobe patterns using the IFT method is capable of handling rectangular or triangular lattices with row displacements. The ultra-low sidelobe results of the three Examples clearly demonstrate that the IFT method can do so. It is also worth noting that it is almost 100% certain that the problem of a limited number far-out sidelobes exceeding the ultra-low sidelobe requirements by a few dB can be completely solved.

It is evident from [4, 5] that planar arrays with a deformed rectangular lattice are quite well suited for limited scan applications, even when using sub-arrays. It is not shown here, but the IFT pattern synthesis method can be applied to arrays equipped with subarrays to find optimum tapers for low sidelobes.

Detailed information about parasitic grating lobes for the three examples, discussed in this paper, can be obtained from the array factor with its main beam pointing at broadside and calculated for the u-v range $\{-2.1 < u < 2.1,$ and $-2.1 < v < 2.1\}$. Even for small arrays having a rectangular or a triangular lattice, many different aperture element configurations can be realized by using variable row displacements. It is therefore likely that some of these configurations will offer an improved scan range by suppressing parasitic grating lobes or shifting them away from the main lobe.

The way parasitic grating lobes are produced and changed due to variable row displacements is not the topic of this manuscript and is therefore not investigated.

A study has been started to solve the problem that some sidelobes located outside the *AFuv* area in u-v space exceed with a few dB the required sidelobe level.

The reported low sidelobe pattern results have been obtained with a PC equipped with an Intel Core i9-12900K processor provided with 32 GB RAM. The MATLAB program used for the IFT low sidelobe pattern synthesis is version R2024b.

REFERENCES

[1] Keizer, W. P. M. N., "Low sidelobe pattern synthesis of array antennas with a triangular or skew lattice using the IFT method," *IEEE Open Journal of Antennas and Propagation*, Vol. 4, 1000–1015, 2023.

[2] Keizer, W. P. M. N., "Affine transformation for synthesis of low sidelobe patterns in planar array antennas with a triangular element grid using the IFT method," *IET Microwaves, Antennas & Propagation*, Vol. 14, No. 8, 830–834, 2020.

[3] Mailloux, R. J., *Phased Array Handbook*, 2nd ed., 84–87, Artech House Inc., Norwood, MA, 2005.

[4] Mailloux, R. J., "Wideband quantization lobe suppression in arrays of columns for limited field of view (LFOV) scanning," in *2015 IEEE International Symposium on Antennas and Propagation & USNC/URSI National Radio Science Meeting*, 2453–2454, Vancouver, BC, Canada, Jul. 2015.

[5] Wang, H., D.-G. Fang, and Y. L. Chow, "Grating lobe reduction in a phased array of limited scanning," *IEEE Transactions on Antennas and Propagation*, Vol. 56, No. 6, 1581–1586, Jun. 2008.

[6] Patton, W. T. and L. H. Yorinks, "Near-field alignment of phased-array antennas," *IEEE Transactions on Antennas and Propagation*, Vol. 47, No. 3, 584–591, Mar. 1999.

[7] Keizer, W. P. M. N., "Synthesis of scan- and frequency-invariant low-sidelobe tapers for planar array antennas," *IEEE Transactions on Antennas and Propagation*, Vol. 64, No. 8, 3703–3707, Aug. 2016.